Molecular fingerprinting of wetland organic matter using pyrolysis GC/MS: an example from the southern Cape coastline of South Africa

Andrew S Carr[1], Arnoud Boom[1], Brian M Chase[2], David L Roberts[3], Zoë E Roberts[1]

[1]Department of Geography, University of Leicester, UK; asc18@le.ac.uk; ab269@le.ac.uk

[2]Department of Archaeology, History, Cultural Studies and Religion, University of Bergen, 5020 Bergen, Norway Brian.Chase@ahkr.uib.no and Institut des Sciences de l'Evolution de Montpellier, UMR 5554, Centre National de Recherche Scientifique/Université Montpellier 2, Bat.22, CC061, Place Eugène Bataillon, 34095 Montpellier, cedex5, France

[3]Council for Geoscience, Cape Town, South Africa; droberts@geoscience.org.za

Keywords: Py-GC/MS; Biomarker; Quaternary, Diagenesis; Lignin

Published in Journal of Paleolimnology 44 (4)

Abstract

Pyrolysis-gas chromatography mass spectrometry (py-GC/MS) allows the characterisation of complex macromolecular organic matter. In lakes and wetlands this can potentially be used to assess the preservation/diagenesis and provenance of sediment organic matter. It can complement palaeoenvironmental investigations utilising 'bulk' sediment variables such as total organic carbon (TOC) and TOC/total nitrogen ratios. We applied py-GC/MS analyses to a ~32,000-year sediment record from the southern Cape coastline of South Africa. We used the results to evaluate the sources and extent of degradation of organic matter in this semi-arid environment.

Marked down-core changes in the relative abundance of multiple pyrolysis products were observed. Correspondence analysis revealed that the major driver of this down-core variability in OM composition was selective preservation/degradation. Samples comprising highly degraded OM are primarily confined to the lower half of the core, older than ~12,000 years, and are characterised by suites of low-molecular-weight aromatic pyrolysis products. Samples rich in organic matter, e.g. surface sediments, are characterised by products derived from fresh emergent or terrestrial vegetation, which include lignin monomers, plant-derived fatty acids and long-chain *n*-alkanes. Pyrolysates from the late glacial-early Holocene period, approximately mid-way down the core are characterised by distinct suites of long-chain *n*-alkene/*n*-alkane doublets, which may reflect the selective preservation of recalcitrant aliphatic macromolecules and/or enhanced inputs of the algal macromolecule algaenan/polymerised algal lipids. Increased TOC, lower $\delta^{13}C$ and increased abundance of more labile lignin and fatty acid products at the same depths suggest this period was associated with increased lake primary productivity and enhanced inputs of terrestrial OM. TOC is the only 'bulk' parameter correlated with the correspondence analysis axes extracted from the py-GC/MS data. Distinct fluctuations in TOC/total nitrogen ratio are not explained by variation in organo-nitrogen pyrolysis products. Notwithstanding, the study suggests that py-GC/MS has potential to complement palaeolimnological investigations, particularly in regions such as southern Africa, where other paleoenvironmental proxy variables in sediments may be lacking or equivocal.

Introduction

Biomarkers preserved in sediments can provide important insights into the origins and fate of sedimentary organic matter (OM). It has long been recognised that different types of biomarkers or classes of organic compounds are subject to more rapid degradation than others. Various recalcitrant biomarkers or polymeric macromolecules, which may be preferentially preserved over time, have been identified within long-term sediment archives (de Leeuw et al. 2006). Given that specific sources of such molecules can sometimes be identified (Kögel-Knabner 2002), such biomarkers can contribute to multi-proxy palaeoenvironmental studies. Pyrolysis-gas chromatography mass spectrometry (py-GC/MS) is a common means by which such macromolecular OM is characterised. With this method, the OM of a sample is thermally degraded to GC-amenable fragments, generating potentially complex, multifaceted datasets (van Smeerdijk and Boon 1987; Saiz-Jimenez and de Leeuw 1987). Data interpretation is not as straightforward as conventional lipid biomarker analyses, as the original macromolecular components must be inferred from the resulting pyrolysis products. Extractable lipids, however, which are more commonly studied, usually comprise a small proportion of the total OM within soils and sediments, whereas py-GC/MS considers a much larger fraction of the sample OM, potentially allowing identification of a range of environmentally-sensitive variables. For example, the technique has been used to characterise the occurrence and type of lignin (Fuhrmann et al. 2003; Vancampenhout et al. 2008), or fire events/black carbon presence (Kaal et al. 2009).

With some exceptions (Bourdon et al. 2000; Fuhrmann et al. 2003, 2004; Vancampenhout et al. 2008), py-GC/MS is used relatively infrequently in multi-disciplinary Quaternary palaeoenvironmental reconstructions, despite having potential to assist the interpretation of bulk organic matter variables (e.g. total organic carbon [TOC], total nitrogen [TN], and $\delta^{13}C_{TOC}$) in long lake sediment sequences. To apply this technique routinely as a palaeoenvironmental tool requires a thorough understanding of the mechanisms governing organic matter preservation and degradation as recorded by py-GC/MS.

Schellekens et al. (2009) recently analysed samples in a 13,000-year peat bog sequence from Tierro Del Fuego and identified key pyrolysis signatures indicative of vegetation change, as well as both aerobic and anaerobic degradation processes. These included the relative significance of lignin monomers (vegetation change) and the abundance and composition of polysaccharide pyrolysis products (degradation). Similarly, Zang and Hatcher (2002) observed systematic down-core changes in pyrolysate composition through a 9,000-year lake sediment sequence from Bermuda. They observed the progressive and selective enrichment of aliphatic pyrolysis products (long-chain carbon

molecules, such as *n*-alkanes and *n*-alkenes) relative to protein and carbohydrate-derived products. A variety of studies have also considered py-GC/MS data obtained from soils (van Bergen et al., 1997; Nierop 1998; Buurman et al. 2005, 2007) and palaeosols (Lui and Huang 2008; Vancampenhout et al. 2008). Using this approach, Vancampenhout et al. (2008) inferred mechanisms of OM degradation and palaeo-vegetation composition through a sequence of loess palaeosols spanning the period 130-70 ka.

Overall, these studies suggest that there is a suite of commonly detected and environmentally sensitive pyrolysis products indicative of plant, algal and microbial contributions to the organic matter pool. Various organic matter fractions show different resistance to degradation, and the susceptibility of cellulose and protein-derived OM in particular has been reported on a number of occasions (Huang et al. 1998; Nierop et al. 2001). The majority of pyrolysis studies thus far have been conducted in humid-temperate environments, where organic matter preservation is enhanced by cool, often water-logged (anaerobic) conditions, and/or have focused on soil OM (Buurman et al. 2007). Vancampenhout et al. (2009) recently demonstrated systematic differences in soil pyrolysis products associated with distinct climates and biomes. Similarly, Bourdon et al. (2000) used py-GC/MS to elucidate the rapid and selective degradation of OM in tropical wetlands of Madagascar. In general however, the composition and degradation of OM in sub-humid to semi-arid environments has received little study. Here we assess the potential of py-GC/MS to provide insights into long-term organic matter preservation and environmental change using a case study from semi-arid southern Africa. We measured OM characteristics in a ~32,000-year wetland sediment core from the southern Cape coastline of South Africa, a region where traditional palaeoecological evidence is sparse (Chase and Meadows 2007). We also sought to identify elements of the py-GC/MS data set that provide new or supplementary insights into local environmental conditions. The aims of the study were to:

1. Characterise down-core variability in organic matter composition and OM preservation using py-GC/MS.
2. Assess key down-core changes in OM provenance within this semi-arid setting.
3. Interpret standard bulk geochemical variables (TOC, TOC/TN and $\delta^{13}C_{TOC}$) in light of the molecular data provided by the py-GC/MS approach.
4. Outline diagnostic elements within the pyrolysis dataset for palaeolimnological and regional palaeoenvironmental reconstructions.

Study location and sample site

Despite a long history of research, palaeoecological data from southern Africa are scarce and fragmentary (Chase and Meadows 2007). This is primarily a function of the relative aridity of large parts of the subcontinent. Much of western southern Africa is arid to semi-arid, which favours the rapid aerobic degradation of organic matter, and lakes or wetlands are rare. Those that do occur represent potentially important palaeoenvironmental archives.

The investigated site is a coastal wetland on the southern Cape of South Africa, ~8 km east of the town of Still Bay (Fig. 1). Rainfall is year-round, but amounts to only ~430 mm a^{-1} and the climate is classified as semi-arid. Rebelo et al. (1991) provide a detailed overview of the contemporary vegetation communities in the Still Bay area, which primarily comprise shrubby *fynbos* ('fine bush') and *renosterveld* elements of the highly diverse and endemic-rich Cape Floristic Region. In addition, the area is characterised by forest/thicket and Karooid communities (Rebelo et al. 1991). With increasing rainfall to the east, there is a greater abundance of southern Cape temperate forests and around the Knysna area, Afromontane forest (Martin 1968). The site's geomorphic history was recently considered in detail by Roberts et al. (2008). The sampled wetland, Rietvlei, occupies a hollow between the landward edge of a last interglacial (125 ka) barrier dune system and the seaward edge of an older barrier dune (Fig. S1). Rietvlei is elongate parallel to the shore, is approximately 3 km in length and averages ~100 m wide. It is extensively covered by a floating mat of emergent vegetation, dominated by *Phragmites australis*. In this respect, the site bears some similarities to the Vankervelsvlei wetland, close to the town of Knysna (Fig. 1), described by Irving and Meadows (1997) further east along this coastline.

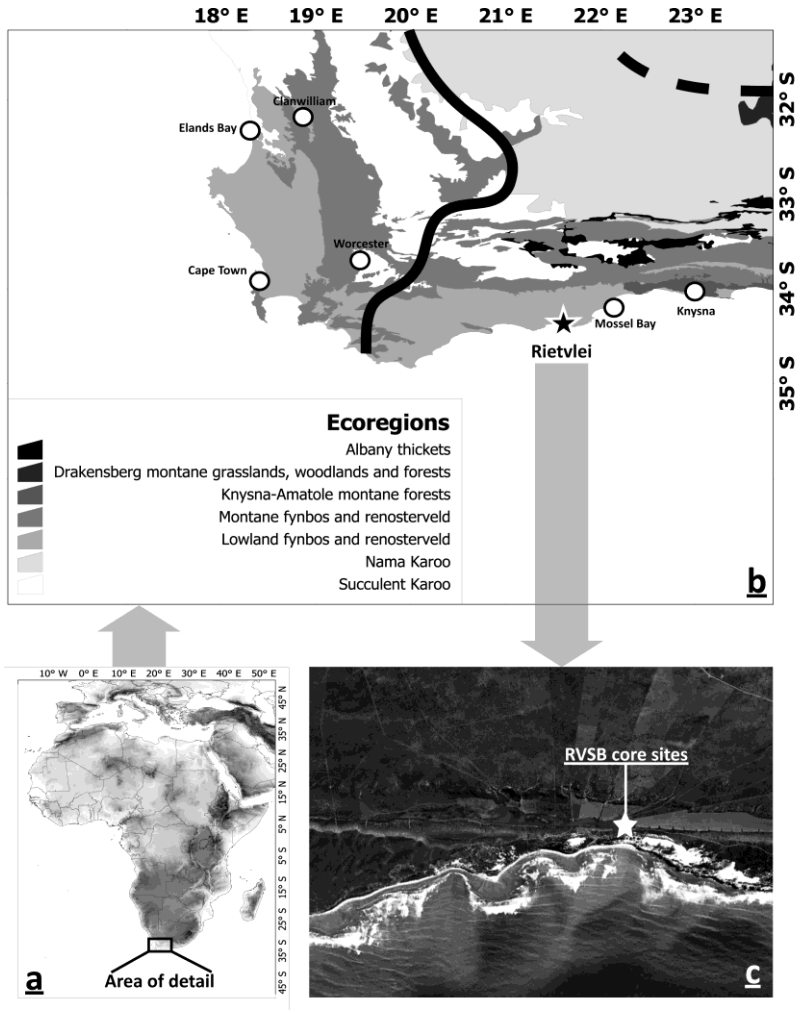

Fig. 1 Location of the Rietvlei site on the southern Cape coastline. This section of the coast lies in a transitional zone between the winter-rainfall environments centred on Cape Town (west of the solid black line) and the summer-rainfall zone, which occupies much of the remainder of South Africa (northeast of the dashed black line). An aerial photo of the wetland is shown in the right inset, with the coring location marked

Materials and methods

Core extraction and chronology

A 3.60-m-long core (RVSB2) was extracted from the eastern margin (Figs. 1 and S1) of the site using a vibracorer (Lanesky et al. 1979). The ends of the core were sealed in the field and the core was split lengthwise in the laboratory at the University of Cape Town. Following sub-sampling, all samples were freeze-dried and homogenised in a ball mill. Three conventional radiocarbon ages provide initial age constraints on the core and were determined at the Department of Geosciences,

University of Arizona using gas proportional counting. The resulting ages were calibrated using the Calib 6.0 software (Stuiver and Reimer 1993) with the SHCal04 Southern Hemisphere Calibration curve (McCormac et al. 2004; samples A- 14938 and A-14939) and the IntCAL09 dataset (Reimer et al. 2009; sample A-14937), which was adjusted for the Southern Hemisphere offset (MCormac et al. 2004). These data, including the 2-sigma calibrated age ranges, are presented in Table 1.

Total organic carbon, total nitrogen and $\delta^{13}C$ measurements

TOC, TN and $\delta^{13}C_{TOC}$ were determined using a SerCon ANCA GSL elemental analyser interfaced to a SerCon Hydra 20-20 continuous flow isotope ratio mass spectrometer. Given the presence of coastal dune-derived carbonate within the sediments, TOC and $\delta^{13}C_{TOC}$ were determined after pre-treatment with 10% hydrochloric acid. All analyses were carried out in triplicate with a typical precision of 0.05 ‰. The data are presented in Fig. 2.

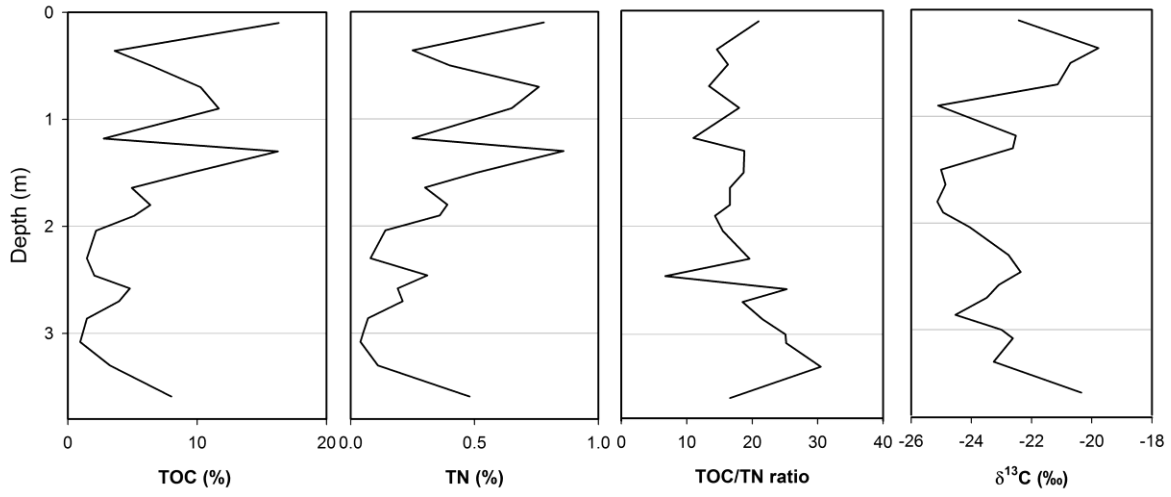

Fig. 2 Down-core variation in total organic carbon (TOC), total nitrogen (TN), TOC/TN and $\delta^{13}C_{TOC}$

Pyrolysis GC/MS (py-GC/MS)

Twenty-one untreated sub-samples of the core were subject to py-GC/MS analyses using a CDS 1000 pyroprobe interfaced with a Perkin Elmer Clarus 500 GC/MS system with a heated (310°C) transfer line. Approximately 0.5 mg of sample was encapsulated in a clean quartz tube and held in place with quartz wool plugs. All samples were inserted into the interface and left for 2 minutes prior to analysis, during which time they were warmed to the system inlet temperature of 310°C. This resulted in the thermal extraction of most free lipids prior to analysis, which was confirmed via

comparison with sub-samples previously subject to total lipid extractions (3xmethanol, 3xDCM [dichloromethane], and 3xhexane with ultrasonic agitation). The samples were pyrolysed at 610°C for 15 seconds. Gas chromatography mass spectrometry was carried out using a CP-Sil 5CB MS column (30 m x 0.25 mm x 320μm). The GC temperature programme comprised an initial temperature of 40°C for 1.8 minutes, which was ramped to a final temperature of 310°C at 4°C min^{-1}. The temperature was then held at 310°C for a further 20 minutes of analysis time. The compounds within the pyrograms were identified based on their mass spectra and retention times. Following compound identification, peak integrations on the total ion current (TIC) were performed using Turbo-Mass 5.2.0 software. The relative abundance of each identified compound was then determined from the ratio of the individual compound integrations to the summed integrations of all identified compounds, following Vancampenhout et al. (2008). To assess compositional variation in a more concise manner and assist interpretation (isolating key indicator compounds influencing sample composition throughout the sequence), data were subjected to multivariate analysis, specifically de-trended correspondence analysis (ter Braak 1995). In addition, selected samples were analysed following the application of an online methylating agent, tetramethyl ammonium hydroxide (TMAH). The resulting methylation prevents complete thermal degradation of some compounds, assisting with the interpretation of the original macromolecular composition of a sample.

Results

Core stratigraphy and chronology

The core comprises a relatively homogenous sequence of slightly silty sands (Fig. S2), with minor increases in silt and clay content at ~1.3 and 2.7-3.0 m. The inorganic sediment fraction is composed primarily of sand-sized, angular to sub-rounded quartz grains, with abundant rounded fragments of mollusc shells and marine micro-fauna, which are derived from the coastal dunes immediately south of site. The upper 0.5 m of the core contained some identifiable plant macro-remains, notably fragments of *Phragmites australis*. The calibrated radiocarbon ages (Table 1) reveal the core to span the period 32,280 cal yr BP (3.5 m; A-14937) to 1,130 cal yr BP (0.88 m; A-14939). The core records the Pleistocene-Holocene transition, with the sample from 2.55 m dating to 11,870 cal yr BP (A-14938). The age-depth model indicates an increase in sedimentation rate in the upper 2.5 m of the core. Although of low resolution, the age model provides sufficient constraints to consider the

detection of, and variability in, down-core OM preservation and provenance, which is the primary aim of this study. Some evidence of minor oxidation (orange mottling) is observed within the lower section of the core at ~3.00 m, and implies shallow-water conditions or sub-aerial exposure of the sediment at this time. A depositional hiatus within this section of the core cannot be ruled out.

Bulk sample TOC, TN and $\delta^{13}C$ data

The TOC content of the core varies between 1 and 16 % (Fig. 2). In general, TOC is highest in the upper 2 m the core, although there is significant variability, including notable reductions in TOC at 1.18 and 0.36 m. The most significant long-term trend corresponds to a down-core reduction in TOC and TOC variability between 2.0 and 3.0 m (typically 1-4 % TOC). TOC subsequently rises to ~8 % between 3.0 m and 3.59 m, near the base of the core. TN follows a similar trend to TOC, varying between 0.1 and 1.0% throughout the core. The TOC/TN ratios vary between 6 and 31 (Fig. 2). The upper 2 m of the core is characterised by fairly constant ratios, which fluctuate between 14 and 20, with a decline to 11 at 1.18 m. Following a brief drop to ~6 at 2.46 m, TOC/TN rises steadily to a core maximum of 31 at 3.3 m, before dropping to 17 at the base of the core. The bulk $\delta^{13}C_{TOC}$ data vary over a range of 5.3 ‰. The lower half of the core (2.0-3.6 m), with the exception of the sample at 3.59 m, varies between -22 and -24 ‰. The core minimum $\delta^{13}C_{TOC}$ (-25.1 ‰) is attained in the middle section of the core between depths of 0.9 and 2.0 m (except at 1.18 m). The upper 1 m of the core is characterised by variable $\delta^{13}C_{TOC}$ values, with notably enriched samples at 0.36 m (-19 ‰) and 0.7 m (-21 ‰).

Pyrolysis GC/MS

A total of 115 pyrolysis products were identified within the Rietvlei samples. These are listed along with their typical retention times in Table S1. Figure 3 shows three example pyrograms. The pyrolysis products fall into the following categories: aromatics (Ar), phenols (Ph), lignin derivatives (Lg), polysaccharide derivatives (Ps), polyaromatic hydrocarbons (PAHs) organo-nitrogen compounds (N), fatty acids (FA), aliphatics (labelled by chain length) and hopanes (HOP). Given their abundance, and the range of potential sources, the aliphatic category was separated into short (up to C_{12}), medium (C_{13}-C_{26}) and long-chain (C_{27}-C_{32}) groups (Fig. 4). The total number of identified compounds in any one sample ranges between 115 and 43, and generally the diversity of detected compounds,

particularly for the polysaccharide and organo-nitrogen compound classes, is lower than that reported in other pyrolysis studies (Buurman et al. 2007; Schellekens et al. 2009).

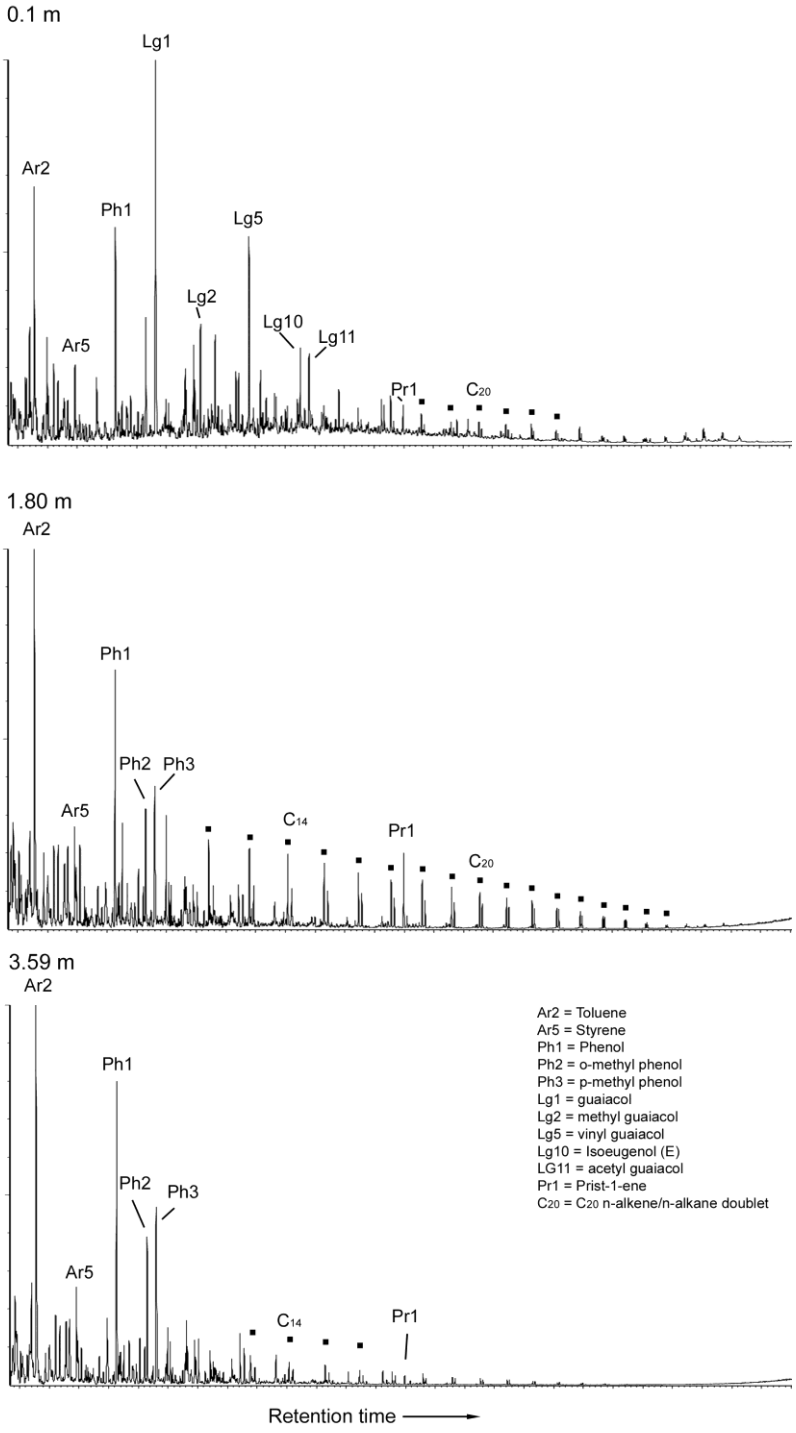

Fig. 3 Example pyrograms from RVSB2. The middle pyrogram (1.8 m) displays a distinct aliphatic signal comprising long-chain *n*-alkene/*n*-alkane doublets and is typical of samples from depths of 0.7-2.04 m. The lowermost example (3.59 m) reveals a far more limited range of pyrolysis products, dominated by aromatic compounds

Sample RVSB-10 (0.1 m) contains by far the highest abundance of aromatic and lignin-derived (29 % of TIC) pyrolysis products (Fig. 4). The lignin pyrolysis products include products of all three lignin precursor monomers (p-coumaryl, coniferyl and sinapyl alcohols). Sinapyl-derived pyrolysis products are minor components in most samples, except at 3.00 m and 3.59 m, whereas coniferyl-derived products are dominated by guaiacol (Lg1), with alkylated guaiacol units (methyl guaiacol [Lg2], ethyl guaiacol [Lg4]) less abundant and declining more rapidly in abundance than guaiacol, down-core. The relative proportion of total lignin-derived products declines abruptly between 0.1 and 0.5 m, markedly increases between 1.30 and 1.90 m (~1-12% of TIC), subsequently drops to <0.3 % of TIC between 2.30-3.30 m, before recovering to 1.3 % at 3.59 m (Fig. 4).

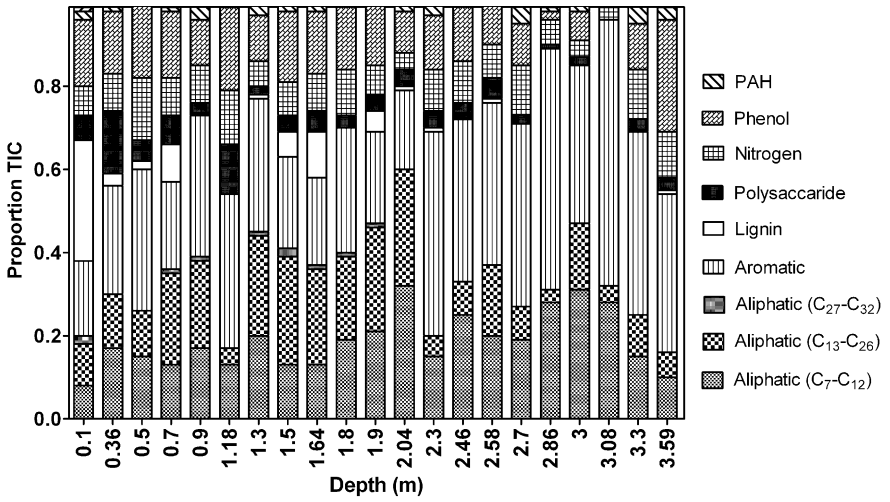

Fig. 4 Relative proportions of the different classes of pyrolysis products identified in the Rietvlei core. For clarity the aliphatic products are sub-divided into short (C_7-C_{12}), medium (C_{13}-C_{26}) and long (C_{27}-C_{32}) chains

For the samples between 0.70 and 2.04 m, there is a distinct increase in the prominence of aliphatic compounds, and more specifically, the medium-chain-length aliphatics (C_{13}-C_{26}). In these samples the C_{13}-C_{26} *n*-alkene/*n*-alkane doublets comprise ~20-28 % of the TIC. Below 2.04 m they represent ~5-17 % of the TIC. The maximum detectable chain length is also variable, ranging from C_{32} (0.1 m) to C_{18} (2.86 m). For the upper 2.04 m, maximum chain lengths vary between C_{24} and C_{32} (average of C_{30}). This drops to between C_{18} and C_{28} (average of C_{24}) in the lower half of the core (2.04-3.30). The application of TMAH to the aliphatic-rich samples produces pyrolysates dominated by a suite of fatty acid methyl esters ranging in chain length from C_6 to C_{32}, but dominated by C_{16} and C_{18} chain lengths (Fig. S3).

A number of fatty acid homologues of chain lengths FA_{16} - FA_{24} were also detected. These are most abundant in the upper 0.7 m. They are characterised by strong even over odd chain length preference, with FA_{16} the dominant homologue. Fatty acids are entirely absent below 2.30 m. Prist-1-ene and prist-2-ene are believed to be produced by the pyrolytic cleavage of chlorophyll-a (Ishiwatari et al. 1991) and are common pyrolysis products of immature kerogens. In RVSB2, prist-1-ene is found in low concentrations (0.01 - 0.2 % TIC) below 2 m, and shows a prominent peak in abundance between 1.3 and 1.9 m (1.6-2.8 % TIC).

Organo-nitrogen compounds (e.g. (methyl) pyrrole, (methyl) pyridine, (methyl) indole, benzonitrile) are present throughout the core and display relatively little change down core (Fig. 4). These are often considered to be pyrolysis products of amino acids (Bracewell and Robertson 1984), although indole has been specifically associated with un-degraded plant matter (Buurman et al. 2007; Verde et al. 2008). Of the organo-nitrogen compounds, only indole (N8) and methyl indole (N9) exhibit down-core trends commensurate with the TOC and TN trends. Polyaromatic hydrocarbons mostly comprise (methyl) naphthalene (PAH 1 and PAH2) and fluorene (PAH 4). Overall, these represent between 0.3 and 4.6 % of the TIC and exhibit no consistent down-core trends (Fig. 4). The polysaccharide-derived compounds include 3-methyl furan (Ps1), furaldehyde (Ps2), (5H)-furan-2-one (Ps3), and acetyl furan (Ps4). Trace amounts (m/z 60+73) of the high molecular weight sugar levoglucosan were found in a limited number of samples (0.10 m, 0.70 m 1.64 m, 2.30 m), but in concentrations too low for peak integration. Hopanes occurred only in samples from the upper 1.8 m. These compounds (22,29,30-Trisnorhop-17(21)-ene, 17β,22,29,30-Trisnorhopane, 17β,21α-30-Normoretane) are typically bacterially-derived membrane lipids. They are also found in lipid extracts from the same samples (data not shown), and given the assumed thermal extraction in the system inlet, the hopanes within the pyrolysate are inferred to have been bound or physically encapsulated within the OM matrix.

Multivariate analysis

Previously, factor analysis has been applied to assess the controls on compositional variation within complex py-GC/MS datasets (Buurman et al. 2007; Vancampenhout et al. 2008 Schellekens et al. 2009). Such multivariate techniques allow the identification of a number of uncorrelated (orthogonal) variables that account for the variation within large datasets. Factor analysis (principal components), however, assumes linear relationships between species (or in this case, compounds) and underlying environmental variables. For this reason correspondence analysis (CA) or related

techniques (de-trended correspondence analysis; DCA) are more commonly applied to environmental and palaeoecological data (ter Braak 1995). Here we apply DCA to the Rietvlei dataset, although we note that PCA analysis (factor analysis following Vancampenhout et al. 2008) places the samples into highly comparable clusters, implying the same fundamental differences between the samples. Analyses were carried out using all untreated samples and all of the resulting data, i.e. 115 compounds.

The DCA ordination diagram for the Rietvlei samples is shown in Fig. 5. The first axis separates the top of the core (right) from the basal section of the core (left) and broad segregation of samples from the upper 2 m of the core (0.1, 0.7, 0.9, 1.3, 1.5, 1.64, 1.8, 1.9, 2.04, along with 2.58 and 3.00) from the lower 1.5 m of the core (2.3, 2.46, 2.7, 2.86, 3.08, 3.3) is apparent. The upper part of the diagram shows a scatter of samples less related to one another stratigraphically; namely 0.36, 0.5, 1.18 and 3.59. To the lower right of the diagram, a notable cluster of samples comprising 0.7, 1.5, 1.64 and 1.9 m, can also be seen. Overall, axis 1 confirms a distinct compositional difference between the top of the core, as might be anticipated for near-modern organic matter, and the lower ~1.5 m of the core. Axis 2 strongly separates sample 2.04 m from sample 1.18 m, and also separates two samples (0.36 and 0.5 m) from the remainder of the upper core samples, which are generally confined to the centre/lower right of the diagram.

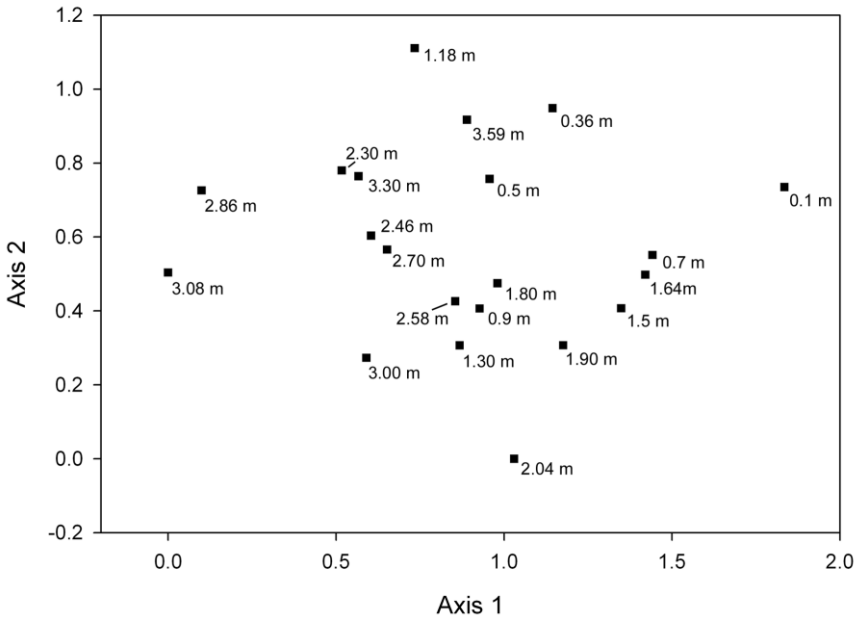

Fig. 5 DCA axes sample scores. Note the separation of fresh organic matter (0.1 m) and the division of the upper from the lower core. Associated eigenvalues: Axis 1 = 0.21, Axis 2 = 0.06

The ordination plot with the individual compound scores provides an indication of the specific compositional variation separating the samples (Fig. 6). Most prominent are the lignin

monomers, which are all found towards the right of the diagram, and are clearly associated with sample 0.1 m, as expected from the description of the pyrograms (Figs. 3 and 4). Also among this cluster are the even-number chain length (FA_{16}-FA_{24}) fatty acids and *n*-alkene/*n*-alkane homologues between C_{29} and C_{31}. Low-molecular-weight aromatic compounds are found to the extreme left of the diagram, and are most closely associated with samples from 2.86 and 3.08 m. These include benzene (Ar1), propyl benzene (Ar8), benzonitrile (N5), indene (Ar10), biphenyl (Ar12), toluene (Ar2), *o*-xylene (Ar4) and *p*-xylene (Ar6). Along the base of the diagram is a series of *n*-alkenes and *n*-alkanes, which display a progressive reduction in chain length from right to left. The longest *n*-alkane/*n*-alkenes ($C_{29:1}$, C_{29}, $C_{30:1}$, C_{30}, $C_{31:1}$ and C_{31}) are associated with the lignin monomers to the right. A prominent cluster of middle-chain-length aliphatics (C_{15}-C_{27}), closely associated prist-1-ene and prist-2-ene, is seen to the lower right. This cluster is most closely associated with the previously noted cluster of samples including 0.7 m, 1.5 m, 1.64 m and 1.9 m. With the exception of N9 (benzonitrile), which plots to the left of the diagram with the aromatics, the organo-nitrogen compounds and all of the polysaccharide products (Ps1 Ps4) all cluster towards the upper centre of the diagram. The separation of samples with high axis 2 scores is seemingly driven in part by the occurrence of secondary cellulose products, furaldehyde (Ps2) and (5H)-furan-2-one (Ps3), although methyl furan (Ps1) also exhibits relatively high axis 2 scores. Polyaromatic compounds mostly plot towards the centre of the diagram, suggesting a limited influence on sample variability. This would be anticipated from the absence of significant down-core trends for these compounds (Fig. 4).

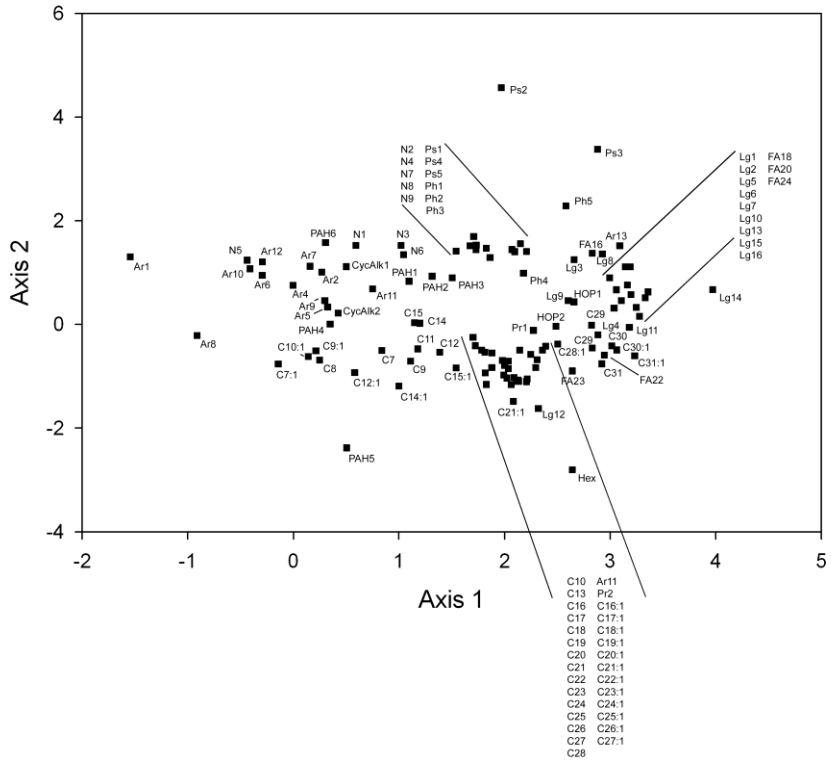

Fig. 6 DCA axes compound scores. The compounds within tight clusters are listed together where necessary

Discussion

In comparison to a number of previous py-GC/MS studies on soils and sediments (van Bergen et al. 1997; Zang and Hatcher 2002; Buurman et al. 2007; Verde et al. 2008; Schellekens et al. 2009; Vancampenhout et al. 2009), the diversity of pyrolysis products in Rietvlei is relatively low. Most notably, compound classes typically associated with the least resistance to degradation (polysaccharide and cellulose pyrolysis products) are present in low concentrations and are of low diversity. The polysaccharide pyrolysis products in particular are dominated by a limited number of moieties from 'secondary' polysaccharides, primarily furans (e.g. 3-methyl furan, acetyl furan) and furaldehyde, which are most likely products of microbial degradation of higher molecular weight polysaccharides (Nierop et al. 2001; Kaal et al. 2007; Schellekens et al. 2009). Primary polysaccharides such as levoglucosan, which is a common pyrolysis product of fresh cellulose, were absent or could only be identified in trace amounts.

Pyrolysate diversity and TOC are closely and non-linearly correlated (r^2 = 0.52; Fig. S4). This relationship is insensitive to analysed sample mass (i.e. adjusted for TOC content), and is inferred to be indicative of degradation processes within this environment, which progressively diminish the range of potential pyrolysis products within a sample. Samples to the left of the ordination plot (2.86 m and 3.08 m) are associated with the lowest TOC contents and the least diverse pyrolysates. Their pyrolysates are dominated by aromatics and short-chain-length *n*-alkenes/*n*-alkanes. Toluene (Ar2) in particular has been associated with heavily degraded organic matter (van Bergen et al. 1997; Schellekens et al. 2009) and may be derived from multiple sources, including degraded proteins (Fuhrmann et al. 2004). Similarly, ethyl benzene (Ar3) has also been observed to increase in abundance with the degradation of proteinaceous material (Nguyen et al. 2003). Despite a range of potential sources, styrene (Ar5), phenol (Ph1) and methyl phenol (Ph2/3) have also been associated with microbial residues (Nierop et al. 2001).

The significance of lignin products on the right of axis 1 implies that this is a dominant fraction of fresh OM. The concentration and diversity of lignin products rapidly declines down core. Notably, alkylated guaiacyl units (methyl guaiacol [Lg2], ethyl guaiacol [Lg4]) and syringol units decline most rapidly (Siaz-Jimenez et al. 1987; Thevenot et al. 2010). This pattern is associated with elimination of methoxy groups, side chain shortening and aerobic degradation (Nierop et al. 2001). It is anticipated that lignin is particularly susceptible to microbial degradation in warm, oxygenated environments. For instance, Bourdon et al. (2000) reported rapid lignin degradation within the upper centimetres of the Lake Tritrivakely marsh sediments. At Rietvlei the pH (7.5) of the lake waters and

sediments, which is a result of the surrounding geology (Roberts et al. 2008), also enhances lignin degradation (Liu and Huang 2008). The relationship between TOC and pyrolysate diversity therefore reflects the selective loss of more labile compound classes (proteins, cellulose and lignin) along with the progressive loss of functional groups and depolymerisation due to microbial activity, all of which serve to reduce the range of potential pyrolysis products.

The DCA analysis reveals that first order differences in sample composition reflect pyrolysates dominated by aromatic compounds (low axis 1 scores) relative to pyrolysates rich in lignin-derived/aliphatic compounds (high axis 1 scores). Axis 1 compound scores are significantly correlated with TOC (r^2 = 0.42, p <0.002, n=21), implying that this axis represents the extent of organic matter preservation. The sample from 0.1 m is characterised by abundant lignin, fatty acids and long-chain (>C_{29}-C_{31}) *n*-alkenes and *n*-alkanes, all of which are indicative of higher plant origin (van Bergen et al. 1997; Huang et al. 1998; Nierop et al. 2001), with leaf waxes probably accounting for the C_{29}-C_{31} *n*-alkenes/*n*-alkanes in this cluster. Such an interpretation corresponds with the present dominance of semi-aquatic *Phragmites australis* vegetation at the site (Fig. S1) and is further supported by the presence of all three lignin monomers, indicative of monocotyledonous lignin sources (Boerjan et al. 2003). As observed in previous py-GC/MS studies (Huang et al. 1998), fatty acid abundance declines rapidly with degradation time/depth.

Positive axis 2 scores are associated with the abundance of secondary cellulose products, primarily furaldehyde. Negative values for axis two are primarily associated with *n*-alkenes/*n*-alkanes, which decrease in chain length from right to left across the diagram, i.e. along axis 1 (Fig. 3). The samples from 0.7 m, 1.5 m, 1.64 m and 1.9 m plot closest to the prominent middle-chain-length aliphatic cluster. In lacustrine contexts, such strongly aliphatic pyrolysates (Fig. 3) have been associated with recalcitrant cell wall biopolymers in green algae (algaenan; Blokker et al. 1998; Bourdon et al. 2000; Furhman et al. 2004). Strongly aliphatic pyrolysis signals have also been reported in soils (Nierop 1998; Augris et al. 1998), plant cuticles (cutan; Boom et al. 2005), and roots (Tegelaar et al. 1995). In this context, an aquatic algal source is a plausible origin, although their positioning within the ordination plot places them on a clear gradation between the fresh organic matter (0.1 m) and the degraded organic matter associated with the left side of the diagram. These aliphatic-rich samples also lie between these end-members stratigraphically, and a plausible interpretation is that the aliphatic signal is indicative of the selective preservation of more recalcitrant aliphatic macromolecular organic matter. While these samples have yet to be degraded to the state of the lower metre of the core, their aliphatic signal is relatively enhanced due to the loss of more labile polysaccharide and lignin OM fractions. In this sense, it is also significant that the aliphatics plot at the end of axis 2, opposite the more labile polysaccharide and organo-nitrogen

pyrolysis products. The selective enhancement of aliphatic pyrolysis products has been reported in a number of contexts (Huang et al. 1998; Zang and Hatcher 2002) and is thought to be an important process over geological timescales (de Leeuw et al. 2006; Zonneveld et al. 2010).

Interestingly however, the same section of the core (2.04-0.9 m) is associated with a marked increase in TOC and a recovery in the relative amount of lignin-derived pyrolysis products (Figs. 2 and 4). In conjunction, there is a distinct reduction in $\delta^{13}C_{TOC}$, while TOC/TN ratios stabilise between ~11 and 18 (Fig. 2). A typical interpretation of the latter values is that they potentially reflect algal-derived OM contributions (TOC/TN typically 4 -10; Meyers 1997). In addition, the suite of fatty acid methyl esters revealed by TMAH analyses of samples from these depths implies a potential source of condensed lipids within the sample OM. These may also be derived from algal lipids (Bourdon et al. 2000; Versteegh et al. 2004). Thus, although selective preservation is implied by the ordination space, a change in organic matter source and/or lake productivity at this time is plausible given the evidence from the bulk measurements, the increased prominence of some other pyrolysis products (e.g. lignin), and the TMAH analyses.

Relationship to TOC, TN and TOC/TN

The ordination sample scores are plotted stratigraphically with TOC and TOC/TN (Fig. 7). Much of the lower core (3.1-2.3 m) is characterised by low TOC, high TOC/TN ratios and low axis 1 scores. This section of the core is associated with heavily degraded organic matter, inferred from axis 1. The mid-core section (2.3-1.3 m) is characterised by rising TOC, rising axis 1 scores, a plateau of lower axis 2 scores, and low-moderate TOC/TN ratios. Similar trends in bulk parameters are often observed in lake sediment records during phases of wetter climate and increased lake productivity. These typically comprise an association of increased TOC, lower TOC/TN and a higher rock-eval hydrogen index (Meyers and Lallier-Vargès 1999). Here, a marked increase in preservation (rising axis 1 score and high TOC) is inferred, while the lower axis 2 scores are associated with increasing prominence of the middle-chain-length aliphatics. Between 1.3 and 0.9 m there is an abrupt decrease in axis 1 scores (increased degradation) and an increase in axis 2 scores, commensurate with a drop in TOC. This is associated with the sample at 1.18 m, which is also separated from the rest of the core in the upper center of the sample ordination diagram (Fig. 5). The section between 0.9 and 0.7 m yields opposite trends (axis 1 and TOC increase while axis 2 decreases), with the cycle repeating over the depths 0.7-0.3 m (lower TOC, reduced preservation), and from 0.3 m to the top of the core (increasing TOC and preservation).

Of the bulk sediment parameters, only TOC shows a significant correlation with the sample ordination axes (Fig. 7). The TOC/TN ratio is frequently used as an indicator of OM provenance in palaeolimnology studies (Meyers and Lallier-Vergès 1999), but shows no statistical relationship with either ordination axis. The marked increase in TOC/TN ratio lower in the core (3.1-2.3 m) is associated with the lowest axis 1 scores (degraded OM) and low TOC. Within lacustrine contexts, such high TOC/TN ratios are often associated with increased terrestrial OM inputs (Lamb et al. 2004). Here, the pyrolysis data only imply a marked reduction in OM preservation, and give little information on provenance at these depths. A plausible interpretation is that the rise in TOC/TN ratio is indicative of the preferential degradation of more labile nitrogenous compounds (Meyers and Lallier-Vergès 1999; Nguyen et al. 2003; Das 2008). The (total) proportion of organo-nitrogen pyrolysis products throughout the core is, however, uncorrelated with TN (r^2 = <0.01) or TOC/TN. The two samples (3.00 and 3.08) with the highest TOC/TN ratios do, however, produce the lowest proportion of organo-nitrogen pyrolysis products. It is possible that the py-GC/MS technique is insensitive to the full range of nitrogen compounds in the samples (Nierop et al. 2001; Kaal et al. 2007), some of which are found early in the pyrogram and are frequently difficult to integrate precisely (Kaal et al. 2007). Overall, in the context of the associated core-wide evidence for substantial and selective OM degradation, it seems plausible that the increase in TOC/TN ratio in the lower core is also at least partly driven by selective degradation. This further implies that down-core variations in bulk TOC/TN ratio may be driven by both preservation and provenance.

A key finding from the py-GC/MS analysis is that fresh organic matter is significantly degraded within the upper 50 cm of the core. This is driven initially by the loss of the plant-derived fatty acids and lignin monomers (Bourdon et al. 2000), with a slower and more variable reduction in the contribution of secondary (degraded/microbially-derived) cellulose. Much of this occurs within 1 m of the surface, i.e. the last ~1100 years. In detail, the overall down-core trend (Fig. S5) in secondary cellulose pyrolysis products reveals peaks at 1.18 m and 0.36 m, depths for which enhanced OM degradation was also inferred from the DCA analysis. These peaks likely indicate an enhanced contribution of microbially processed OM, which accounts for the positioning of samples 1.18 m and 0.36 m within the ordination diagram.

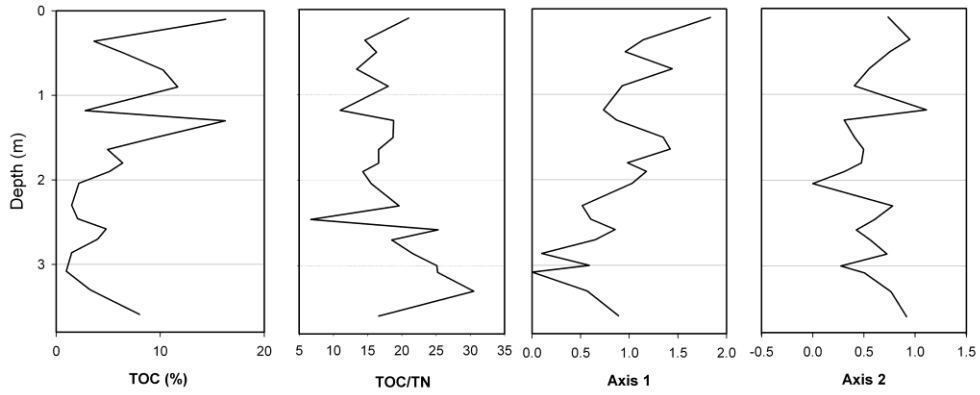

Fig. 7 TOC, TOC/TN, and Axis 1 and Axis 2 sample scores plotted stratigraphically

Regional palaeoenvironmental context

The record preserved in the Rietvlei core spans approximately 32,000 years, a period of time characterised by marked changes in regional environmental conditions (Chase and Meadows 2007). Although regional palaeoenvironmental records are sparse, and the resolution of the Rietvlei core chronology is limited, climate of the southern Cape during the period 32-12 ka is thought to have included phases of relative aridity, notably during the last glacial maximum (Deacon et al. 1984; Irving 1998; Carr et al. 2006). This broadly corresponds with the evidence for highly degraded OM at 2.5 - 3.3 m (32,280 to 11,870 cal yr BP). Subsequently, the late glacial, and most likely the early Holocene (from 11,870 cal yr BP, i.e. samples above 2.5 m), record a notable increase in TOC, a decrease in $\delta^{13}C_{TOC}$, enhanced terrestrial lignin input/preservation and an increase in aliphatic, possibly algal-derived, organic matter. This corresponds with regional evidence for increased moisture availability during the post glacial period (Deacon et al. 1984; Irving 1998). The associated depletion of $\delta^{13}C_{TOC}$ is inferred to have been driven by an increased input of allochthonous organic matter, promoted by a more humid environment. The period prior and subsequent to 1,130 cal yr BP (1.18 m - 0.9 m) displays high, but variable TOC and $\delta^{13}C_{TOC}$. The samples at 1.18 m and 0.36 m are clearly separated by the DCA ordination, driven in part by an increased proportion of secondary polysaccharides and a decrease in lignin/fatty acid products relative to neighbouring samples. These may be associated with phases of relative aridity during the late Holocene, which are apparent in regional palaeoenvironmental records (Scholtz 1986; Carr et al. 2006). Ongoing chronological, palynological and charcoal analyses will allow further comparison of these observations with local/regional palaeoenvironmental records.

Conclusions

Py-GC/MS analyses of the Rietvlei sediments reveal marked fluctuations in organic matter composition. The majority of down-core variation reflects OM preservation, which at its most advanced stage produces pyrolysates dominated by a suite of low-molecular-weight aromatic compounds. The pyrolysis data reveal pronounced, rapid (<1000 years) and selective degradation of OM within this setting. This is supported in the upper core by the low diversity of polysaccharide pyrolysis products (particularly levosugars) and selective degradation of labile organic matter components (polysaccharides, lignin), and in the middle core, by possible selective preservation of aliphatic-rich OM. Lignin monomers and plant-derived fatty acids degrade quickly, whereas the proportion of polysaccharide products declines more slowly over ~1000 years and fluctuates with the addition of bacterially-derived sugars (e.g. 0.36 m). A phase of increased TOC with lower TOC/TN and $\delta^{13}C_{TOC}$ corresponds with the aliphatic-rich pyrolysates, which may reflect selective preservation and/or increased algal-derived organic matter. The timing of this event (from ~12,000 years ago) is broadly consistent with expectations from the regional palaeoenvironmental record. Only DCA axis 1 shows any correlation with 'bulk' OM parameters (TOC). With the exception of (methyl) indole, the organo-nitrogen pyrolysis products provide no insights into the driver(s) of down-core TN or TOC/TN variability. Overall, however, we suggest that in conjunction with bulk sediment parameters, py-GC/MS data can provide useful insights into the origin and preservation of OM within wetland and lake sediment records.

Acknowledgements

We thank Guy Gardener for access to the Rietvlei site and Professor Mike Meadows for use of the vibracorer. ASC thanks the Quaternary Research Association and the University of Leicester for funding the fieldwork associated with this project. The University of Leicester is also thanked for a research sabbatical allocated to ASC, which allowed this work to be completed. ZER is supported by the Leverhulme Trust (Grant F/00 212/AF awarded to ASC). Two reviewers are thanked for very constructive comments on an earlier version of this paper.

References

Augris N, Balesdent J, Mariotti A, Derenne S, Largeau C (1998) Structure and origin of insoluble and non-hydrolyzable, aliphatic organic matter in a forest soil. Org. Geochem 28: 119–124

van Bergen PF, Bull ID, Poulton PR, Evershed RP (1997) Organic geochemical studies of soils from the Rothamsted Classical Experiments I. Total lipids, solvent insoluble residues and humic acids from Broadbalk Wilderness. Org. Geochem 26: 117–135.

Blokker P, Schouten S, Van den Ende H, de Leeuw JW, Hatcher PG, Sinninghe Damsté JS (1998) Chemical structure of algaenans from the fresh water algae *Tetraedron minimum*, *Scenedesmus communis* and *Pediastrum boryanum*. Org. Geochem 29: 1453-1468

Boerjan W, Ralph J, Baucher M, (2003) Lignin biosynthesis. Annu Rev Plant Biol 54: 519-546

Boom A, Sinninghe-Damsté JS, de Leeuw, JW (2005) Cutan, a common aliphatic biopolymer in cuticles of drought-adapted plants. Org. Geochem 36: 595–601.

Bourdon S, Laggoun-Défarge F, Disnar DR, Maman O, Guillet B, Derenne S, Largeau C (2000) Organic matter sources and early diagenetic degradation in a tropical peaty marsh (Tritrivakely, Madagascar). Implications for environmental reconstruction during the Sub-Atlantic. Org. Geochem 31: 421–438

Bracewell JM, Robertson GW (1984) Quantitative comparison of the nitrogen-containing pyrolysis products and amino acid composition of soil humic acids. J Anal Appl Pyrolysis 6: 19-29

Buurman P, van Bergen PF, Jongmans AG, Meijer EL, Duran B, van Lagen B (2005) Spatial and temporal variation in podzel organic matter studied by pyrolysis-gas chromatography/mass spectrometry and micromorphology. Eur J Soil Biol 56: 253-270

Buurman P, Schellekens J, Fritze H, Nierop KGJ, (2007) Selective depletion of organic matter in mottled podzol horizons. Soil Biol Biochem 39: 607–621.

Carr AS, Thomas DSG, Bateman MD, Meadows ME, Chase, BM (2006) Late Quaternary palaeoenvironments of the winter-rainfall zone of southern Africa: palynological and sedimentological evidence from the Agulhas Plain. Palaeogeogr Palaeoclimatol Palaeoecol 239: 147-165.

586 Chase BM, Meadows ME (2007) Late Quaternary dynamics of southern Africa's winter rainfall zone.
587 Earth-Science Reviews 84: 103-138.
588
589 Das SK, Routh J, Roychoudhury AN, Val Klump J (2008) Elemental (C, N, H and P) and stable isotope
590 ($\delta^{15}N$ and $\delta^{13}C$) signatures in sediments from Zeekoevlei, South Africa: a record of human
591 intervention in the lake. J Palaeolimnol 36: 349-360
592
593 Deacon HJ, Deacon J, Scholtz A, Thackeray JF, Brink JS, Vogel JC (1984) Correlation of
594 palaeoenvironmental data from the Late Pleistocene and Holocene deposits at Boomplaas
595 cave, southern Cape. In: Vogel JC (ed), Late Cainozoic Palaeoenvironments of the Southern
596 Hemisphere. AA Balkema, Rotterdam, pp. 339–352.
597
598 Fuhrmann A, Mingram J, Lücke A, Lu H, Horsfield B, Liu J, Negendank JFW, Schleser GH, Wilkes H
599 (2003) Variations in organic matter composition in sediments from Lake Huguang Maar
600 (Huguangyan), south China during the last 68 ka: Implications for environmental and climatic
601 change. Org. Geochem 34: 1497-1515
602
603 Fuhrmann A, Fischer T, Lücke A, Brauer A, Zolitschka B, Horsfield B, Negendank JFW, Schleser GH,
604 Wilkes H. (2004) Late Quaternary environmental and climatic changes in central Europe as
605 inferred from the composition of organic matter in annually laminated maar lake sediments.
606 Geochemistry Geophysics Geosystems 5; Article Number: Q11015
607
608 Huang Y, Stankiewicz BA, Eglinton G, Snape CE, Evans B, Latter PM, Ineson P (1998) Monitoring
609 biomacromolecular degradation of *Calluna vulgaris* in a 23 year field experiment using solid
610 state ^{13}C-NMR and pyrolysis GC/MS. Soil Biol Biochem 30: 1517-1528.
611
612 Irving SJ (1998) Late Quaternary palaeoenvironments at Vankervelsvlei, near Knysna, South Africa.
613 Unpublished MSc thesis, University of Cape Town.
614
615 Irving SJ, Meadows ME (1997) Radiocarbon chronology and organic matter accumulation at
616 Vankervelsvlei, near Knysna, South Africa. South African Geographical Journal 79: 101-105
617

Ishuwatari M, Ishiwatari R, Sakashita H, Tatsumi T, Tominaga H (1991) Pyrolysis of chlorophyll-a after preliminary heating at a moderate temperature: implications for the origins of Prist-1-ene on kerogen pyrolysis. J Anal Appl Pyrolysis 18: 207-218

Kaal J, Baldock JA, Buurman P, Nierop KGJ, Pontevedra-Pombol X, Martínez-Cortizas AM (2007) Evaluating pyrolysis-GC/MS and 13C CPMAS NMR in conjunction with a molecular mixing model of the Penido Vello peat deposit, NW Spain. Org. Geochem 38: 1097-1111

Kaal J, Martinez-Cortizas A, Nierop KGJ (2009) Characterisation of aged charcoal using a coil probe pyrolysis-GC/MS method optimised for black carbon. J Anal Appl Pyrolysis 85: 408-416

Kögel-Knaber I (2002) The macromolecular organic composition of plant and microbial residues as inputs to soil organic matter. Soil Biol Biochem 34: 139–162.

Lamb AL, Leng MJ, Mohammed MU, Lamb HF (2004) Holocene climate and vegetation change in the Main Ethiopian Rift Valley, inferred from the composition (C/N and $\delta^{13}C$) of lacustrine organic matter. Quat Sci Rev 23: 881-891

Lanesky DE, Logan BW, Brown RG, Hine AC (1979) A new approach to portable vibracoring underwater and on land. J Sediment Petrol 49: 654–657

de Leeuw JW. Versteegh GJM, van Bergen PF (2006) Biomacromolecules of algae and plants and their fossil analogues. Plant Ecol 182: 209-233

Liu W, Huang Y (2008) Reconstructing in-situ vegetation dynamics using carbon isotopic composition of biopolymeric residues in the central Chinese Loess Plateau. Chem Geol 249: 348-346

Martin ARH, (1968) Pollen analysis of Groenvlei lake catchments, Knysna. Rev Palaeobot Palynol 7: 107-144.

McCormac FG, Hogg AG, Blackwell PG, Buck CE, Higham TFG, Reimer PJ (2004) SHCal04 Southern Hemisphere calibration, 0-11.0 cal kyr BP. Radiocarbon 46: 1087-1092

Meyers PA, Lallier-Vergés E (1999) Lacustrine sedimentary organic matter records of Late Quaternary palaeoclimates. J Palaeolimnol 21: 345-372.

Nguyen RT, Harvey HR, Zang X, van Heemst JDH, Hetényi M, Hatcher PG (2003) Preservation of algaenan and proteinaceous material during the oxic decay of *Brotryococcus braunii* as revealed by pyrolysis-gas chromatography/mass spectrometry and ^{13}C NMR spectroscopy. Org. Geochem 34: 483-497

Nierop KGJ (1998) Origin of aliphatic compounds in a forest soil. Org. Geochem 29: 1009–1016.

Nierop KGJ, Pulleman MM, Marinissen JCY (2001). Management induced organic matter differentiation in grassland and arable soil: a study using pyrolysis techniques. Soil Biol Biochem 33: 755-764

Rebelo AG, Cowling, RM, Campbell BM, Meadows M (1991) Plant communities of the Riversdale Plain. S Afr J Bot 57: 10-28.

Reimer PJ, Baillie MGL, Bard E, Bayliss A, Beck JW, Blackwell PG, Bronk Ramsey C, Buck CE, Burr GS, Edwards RL, Friedrich M, Grootes PM, Guilderson TP, Hajdas I, Heaton TJ, Hogg AG, Hughen KA, Kaiser KF, Kromer B, McCormac FG, Manning SW, Reimer RW, Richards DA, Southon JR, Talamo S, Turney CSM, van der Plicht J, Weyhenmeyer CE (2009) IntCal09 and Marine09 Radiocarbon Age Calibration Curves, 0–50,000 Years cal BP. Radiocarbon 51: 1111-1150

Roberts D, Murray-Wallace CV, Bateman, MD, Carr AS, Holmes PJ (2008) Fossil elephant trackways, sedimentation and diagenesis in OSL/AAR-dated Late Quaternary coastal aeolianites: Still Bay, South Africa. Palaeogeogr Palaeoclimatol Palaeoecol 257: 261-279

Saiz-Jimenez C, de Leeuw JW (1987) Chemical characterization of soil organic matter fractions by analytical pyrolysis–gas chromatography–mass spectrometry. J Anal Appl Pyrolysis 9: 99–119.

Saiz-Jimenez C, Boon JJ, Hedges JI, Hessels JKC, de Leeuw JW (1987) Chemical characterisation of recent and buried woods by analytical pyrolysis: comparison of pyrolysis data with ^{13}C NMR and wet chemical data *J Anal Appl Pyrolysis* 11: 437-450

Schellekens J, Buurman P, Pontevedra-Pombal X (2009) Selecting parameters for the environmental interpretation of peat molecular chemistry. Org. Geochem 40: 678-691

Scholtz A (1986) Palynological and Palaeobotanical Studies in the Southern Cape. Unpublished MA thesis, University of Stellenbosch.

van Smeerdijk DG, Boon JJ (1987) Characterisation of subfossil *Sphagnum* leaves, rootlets of ericaceae and their peat pyrolysis-high resolution gas chromatography mass spectrometry. *J Anal Appl Pyrolysis* 11: 377–402

Stuiver M, Reimer PJ (1993) Extended ^{14}C data base and revised CALIB 3.0 ^{14}C age calibration program. Radiocarbon 35: 215-230 (version 6.0)

Tegelaar EW, Hollman G, Vandervegt P, De Leeuw JW, Holloway PJ (1995) Chemical characterization of the periderm tissue of some angiosperm species - recognition of an insoluble, nonhydrolyzable, aliphatic biomacromolecule (suberan). Org Geochem 23: 239-251

ter Braak CJF (1995) Ordination. In: Jongman RHG, ter Braak CJF, van Tongeren OFR (Eds). Data analysis in community and landscape ecology. Cambridge Univ. Press, Cambridge, pp 91–173

Thevenot M, Dignac M-F, Rumpel C (2010) Fate of lignin in soils: A review. Soil Biol Biochem 42: 1200-1211

Vancampenhout K, Wouters K, Caus A, Buurman P, Swennen R, Deckers J (2008) Fingerprinting of soil organic matter as a proxy for assessing climate and vegetation changes in last interglacial palaeosols (Veldwezelt, Belgium). Quat Res 69: 145–162

Vancampenhout K, Wouters K, De Vos B, Buurman P, Swennen R, Deckers J (2009) Differences in chemical composition of soil organic matter in natural ecosystems from different climatic regimes – A pyrolysis-GC/MS study. Soil Biol Biochem 41: 568-579

Verde JR, Buurman P, Martínez-Cortizas A, Macías F, Arbestain MC (2008) NaOH-extractable organic matter of andic soils from Galicia (NW Spain) under different land use regimes: a pyrolysis GC/MS study. Eur J Soil Sci 59: 1096-1110

Versteegh GJM, Blokker P, Wood GD, Collinson ME, Sinninghe-Damsté JS, de Leeuw JW (2004) An example of oxidative polymerisation of unsaturated fatty acids as a preservation pathway for dinoflagellate organic matter. Org Geochem 35: 1129-1139

Zang X, Hatcher PG (2002) A py-GC-MS and NMR spectroscopy study of organic nitrogen in Mangrove Lake sediments. Org. Geochem 33: 201-211

Zonneveld KAF, Versteegh GJM, Kasten S, Eglinton TI, Emeis K-C, Huguet C, Koch BP, de Lange GJ, de Leeuw JW, Middelburg JJ, Mollenhauer G, Prahl FG, Rethemeyer J , Wakeham SG (2010) Selective preservation of organic matter in marine environments; processes and impact on the sedimentary record. Biogeosci. 7: 483-511

737 **Tables**

738

739 Table 1. RVSB-2 core radiocarbon ages and calibrated dates. Calibration was conducted with Calib
740 v6.0 using the ShCal04 (A-14939 and A- 14938) and IntCal09 (A- 14937) calibration curves. A
741 Southern Hemisphere correction was applied to A- 14937

Sample	Depth (m)	Method	^{14}C age yr BP	1 σ error (yr)	calibration data	95.4 % (2σ) cal age ranges (cal yr BP)	relative area	median probability (cal yr BP)
A-14939	0.88	GPC	1,260	70	SHCal04	1,274 – 977	1	1,130
A- 14938	2.55	GPC	10,250	120	SHCal04	11,366 – 11,137	0.00159	
						12,245 – 11,393	0.946	11,870
						12,375 – 12,265	0.0525	
A- 14937	3.51	GPC	27,686*	1135*	INTCAL09	34,622 – 30,363	1	32,280

742

743 *Adjusted for recommended SH offset of 56 ± 24
744 GPC = Gas proportional counting
745

746 Supplementary material

747 **Table S1**: Identified compounds within the pyrolysates, approximate retention times, and the coding
748 system used for figures 5 and 6
749

Compound	***Compound code***	***Typical retention time (min)***	***Class***
Cyclohexadiene	CycAlk1	2.67	Aliphatic
Benzene	Ar1	2.86	Aromatic
Cyclohexene	CycAlk2	3.19	Aliphatic
Heptene	C7:1	3.35	Aliphatic
Heptane	C7	3.52	Aliphatic
Pyridine	N1	3.97	Nitrogen
Toluene	Ar2	4.62	Aromatic
C8 alkene	C8	5.42	Aliphatic
3-methyl furan	Ps1	5.72	Polysaccharide
Furaldehyde	Ps2	5.84	Polysaccharide
Methyl pyrrole	N2	6.28	Organo-nitrogen
3-methyl pyrrole	N3	6.64	Organo-nitrogen
2-methyl pyridine	N4	6.75	Organo-nitrogen
Ethyl benzene	Ar3	7.17	Aromatic
o-Xylene	Ar4	7.46	Aromatic
(5H)-furan-2-one	Ps3	7.65	Polysaccharide
Styrene	Ar5	8.07	Aromatic
p-Xylene	Ar6	8.17	Aromatic
Acetyl furan	Ps4	8.30	Polysaccharide
C9 alkene	C9:1	8.46	Aliphatic
C9 alkane	C9	8.84	Aliphatic
3-methyl-2-cyclopenten-1-one	Ps5*	9.90	Organo-nitrogen*
Benzaldehyde	Ar7	9.97	Aromatic
Propyl benzene	Ar8	10.31	Aromatic
Benzonitrile	N5	10.60	Nitrogen
2-Ethyl-1-methyl benzene	Ar9	11.25	Aromatic
Phenol	Ph1	11.47	Phenol
C10 alkene	C10:1	12.03	Aliphatic
C10 alkane	C10	12.42	Aliphatic
Indene	Ar10	13.38	Aromatic
o-methyl phenol	Ph2	14.04	Phenol
3-methyl Benzonitrile	N6	14.45	Nitrogen
p-methyl phenol	Ph3	14.70	Phenol
Guaiacol	Lg1	14.85	Lignin
Benzoacetyl nitrile	N7	15.93	Nitrogen

C11 alkane	C11:1	16.12	Aliphatic
Pentyl benzene	Ar11	17.68	Aromatic
Ethyl phenol	Ph4	18.05	Phenol
Dimethyl phenol	Ph5	18.14	Phenol
Naphthalene	PAH1	18.38	PAH
Methyl guaiacol	Lg2	18.64	Lignin
C12 alkene	C12:1	19.30	Aliphatic
C12 alkane	C12	19.69	Aliphatic
Vinyl phenol	Lg3	19.87	Phenol/ Lignin
Ethyl guaiacol	Lg4	20.63	Lignin
Indole	N8	21.85	Organo-nitrogen
2-methyl naphtalene	PAH2	22.17	PAH
Vinyl guaiacol	Lg5	22.72	Lignin
C13 alkane	C13	23.10	Aliphatic
Syringol	Lg6	23.69	Lignin
Eugenol	Lg7	24.17	Lignin
Methyl indole	N9	24.88	Organo-nitrogen
Biphenyl	Ar12	24.90	Aromatic
Vanillin	Lg8	25.01	Lignin
Isoeugenol (Z)	Lg9	25.79	Lignin
C14 alkene	C14:1	25.95	Aliphatic
C14 alkane	C14	26.25	Aliphatic
Dimethyl naphthalene	PAH3	26.29	PAH
Trimethoxy benzene	Ar13	26.81	Aromatic
Isoeugenol (E)	Lg10	27.05	Lignin
Acetyl guaiacol	Lg11	27.78	Lignin
Vanillic acid methyl ester	Lg12	28.83	Lignin
C15 alkene	C15:1	29.02	Aliphatic
C15 alkane	C15	29.32	Aliphatic
Vinyl syringol	Lg13	30.29	Lignin
Fluorene	PAH4	31.00	PAH
p-methyl cinamic acid	Lg14	31.05	Lignin
Triethyl naphthalene	PAH5	31.12	PAH
C16 alkene	C16:1	31.91	Aliphatic
C16 alkane	C16	32.18	Aliphatic
Allyl syringol	Lg15	34.09	Lignin
Acetyl syringol	Lg16	34.65	Lignin
C17 alkene	C17:1	34.65	Aliphatic
C17 alkane	C17	34.91	Aliphatic
1-Methyl-7-propyl naphthalene	PAH6	35.21	PAH
Prist-1-ene	Pr1	35.71	Aliphatic
Prist-2-ene	Pr2	35.97	Aliphatic
C18 alkene	C18:1	37.25	Aliphatic
C18 alkane	C18	37.49	Aliphatic

C19 alkene	C19:1	39.73	Aliphatic
C19 alkane	C19	39.96	Aliphatic
C16 Fatty acid	FA16	40.24	Fatty Acid
Hexadecanoic acid	Hex	41.17	Aliphatic
C20 alkene	C20:1	42.10	Aliphatic
C20 alkane	C20	42.30	Aliphatic
C21 alkene	C21:1	44.35	Aliphatic
C21 alkane	C21	44.54	Aliphatic
C18 Fatty acid	FA18	44.84	Fatty Acid
C22 alkene	C22:1	46.51	Aliphatic
C22 alkane	C22	46.69	Aliphatic
C23 alkene	C23:1	48.58	Aliphatic
C23 alkane	C23	48.74	Aliphatic
C20 Fatty acid	FA20	49.04	Fatty Acid
C24 alkene	C24:1	50.56	Aliphatic
C24 alkane	C24	50.71	Aliphatic
C25 alkene	C25:1	52.47	Aliphatic
C25 alkane	C25	52.61	Aliphatic
C22 Fatty acid	FA22	52.92	Fatty Acid
C26 alkene	C26:1	54.29	Aliphatic
C26 alkane	C26	54.43	Aliphatic
C23 Fatty acid	FA23	54.74	Fatty Acid
C27 alkene	C27:1	56.06	Aliphatic
C27 alkane	C27	56.19	Aliphatic
C24 Fatty acid	FA24	56.51	Fatty Acid
C28 alkene	C28:1	57.76	Aliphatic
C28 alkane	C28	57.88	Aliphatic
C29 alkene	C29:1	59.40	Aliphatic
C29 alkane	C29	59.51	Aliphatic
22,29,30-Trisnorhop-17(21)-ene	HOP1	59.68	Hopane
17β,22,29,30-Trisnorhopane	HOP2	60.41	Hopane
C30 alkene	C30:1	60.99	Aliphatic
C30 alkane	C30	61.09	Aliphatic
C31 alkene	C31:1	62.53	Aliphatic
C31 alkane	C31	62.62	Aliphatic
17β,21α-30-Normoretane	HOP3	64.01	Hopane

*Ps5 has a structure very close to a furan suggesting a similar source is plausible

753
754 **Supplementary figures**

755
756
757 **Fig. S1**: Panorama of Rietvlei and the coring site looking north from the crest of the seaward-most
758 barrier dune. The approximate position of the core is marked with the red circle. Vehicle near the
759 centre provides scale
760
761

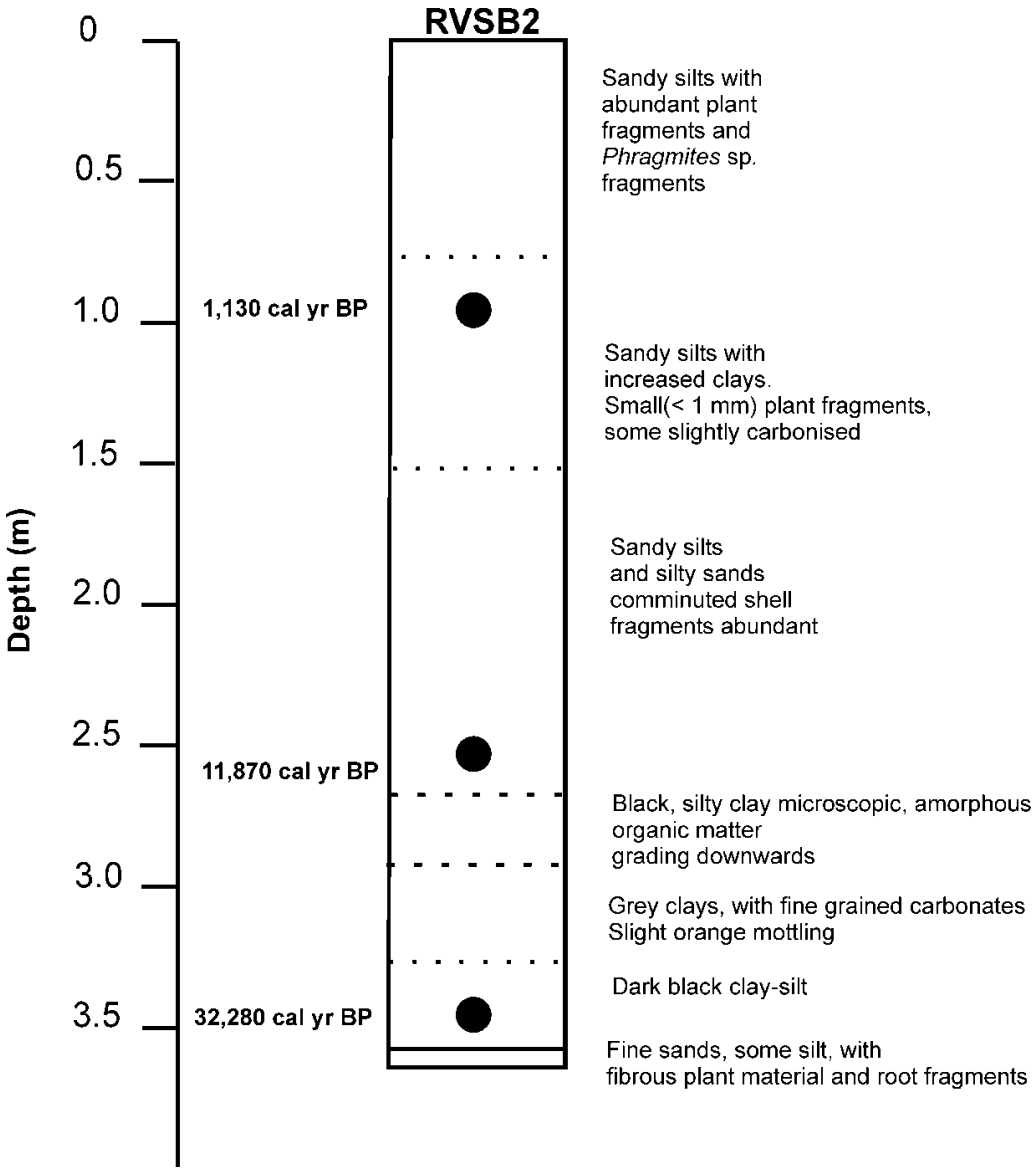

762
763 **Fig. S2:** Simplified core stratigraphy, with median calibrated radiocarbon age ranges shown

764
765

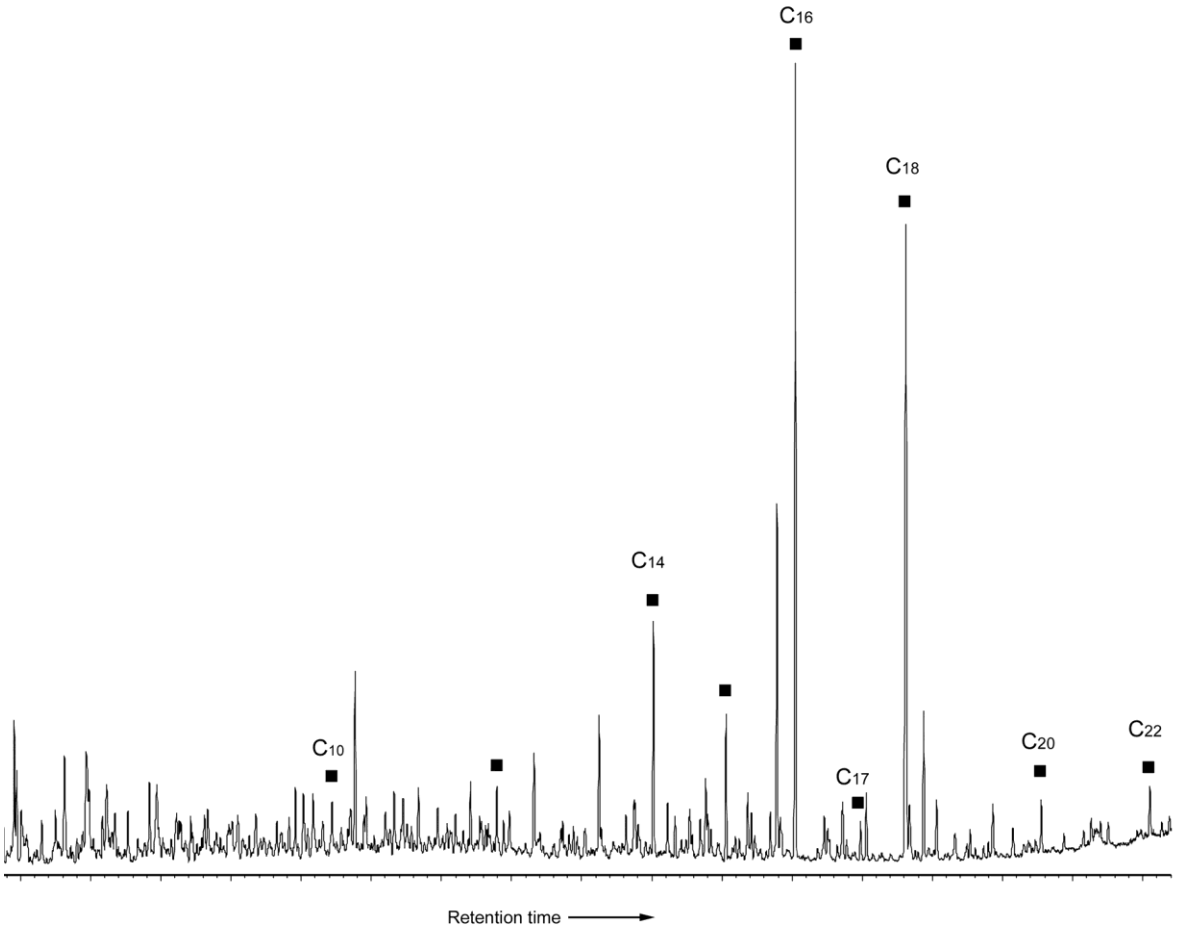

766
767 **Fig. S3**: A partial chromatogram showing the results of TMAH application to an aliphatic rich sample.
768 This example is from 1.8 m depth. Note the dominant C_{16} and C_{18} fatty acid methyl esters
769
770
771
772

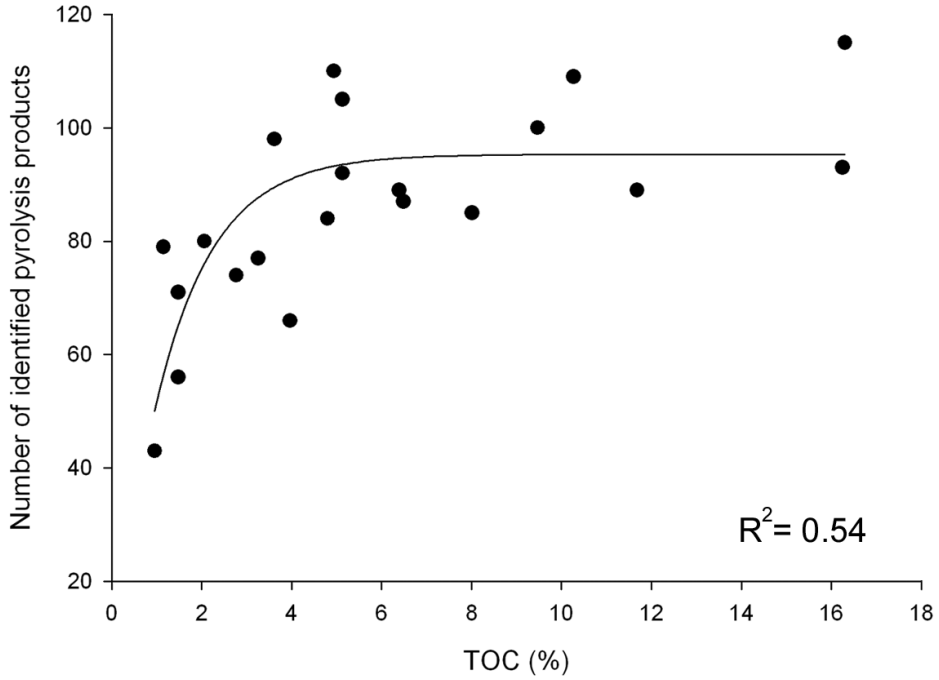

Fig. S4: Relationship of pyrolysate diversity to TOC

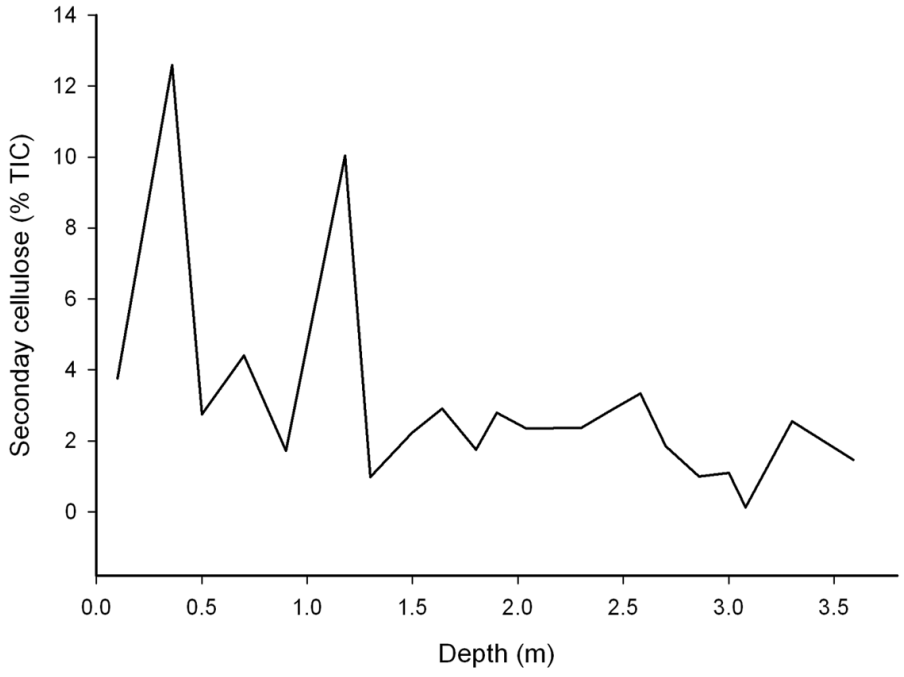

Fig. S5: Down-core concentration of secondary cellulose pyrolysis products (summed proportion of TIC) for 3-methyl furan (Ps1), Furaldehyde (Ps2), (5H)-furan-2-one (Ps3), Acetyl furan (Ps4))